J. Webster (ed.), *Wiley Encyclopedia of Electrical and Electronics Engineering*

MICROWAVE MEASUREMENT INSTRUMENTATION

There are a number of different types of measurements that are carried out at microwave frequencies. These measurements may need to be carried out for the purpose of design and testing, or for research and development. The types of measurements described in this article are:

(1) Microwave radiometry
(2) Microwave spectroscopy
(3) Measurement of permittivity and permeability
(4) Time-domain measurements
(5) Swept-frequency measurement of scattering parameters
(6) Six-port reflectometer
(7) Power measurements

The description here is necessarily brief. More details are available in the references included at the end of the article.

Microwave Radiometry

Microwave radiometry involves measurement of radiant electromagnetic energy in the microwave frequency range (1 GHz to 300 GHz). This energy may be emitted, reflected, or transmitted from or through different media. The objective of these measurements is to infer the physical and/or chemical state of the media such as the earth's atmosphere, land, and sea. Microwave radiometry is also used for astronomical studies and exploration of planetary atmospheres. The term radiometry is often used synonymously with *remote sensing*, typically, *passive remote sensing*; this is also the point of view adopted in this article. Here, we give a simple description, largely based on Ref. 1, of the advantages, physical basis, methodology, and applications of microwave radiometry. There are a number of topics related to radiometry that are considered in detail elsewhere in this encyclopedia. These topics include Radiometry, Remote Sensing by Radar, Microwave Remote Sensing Theory, Microwave Propagation and Scattering for Remote Sensing, Information Processing For Remote Sensing, and Radiometry. There are also a number of excellent references available on microwave radiometry and remote sensing; some of these are listed at the end of this article (1,2,3,4). Current information on this topic is covered in journals such as *IEEE Transactions on Geoscience and Remote Sensing*. The reader can look up these topics and references for a wealth of useful information and details on microwave radiometry.

For remote sensing applications, *optical imaging* at visible frequencies predates microwave radiometry. However, there are certain advantages of using microwave frequencies. First of all, as opposed to optical frequencies, microwaves have the capability to penetrate clouds and, to some extent, rain. This permits an almost all-weather observation capability for both spaceborne and terrestrial radiometric platforms. Secondly,

microwaves are able to penetrate more deeply into vegetation and ground than visible and infrared radiation. The extent of penetration depends upon the wavelength and upon the moisture content and density of the vegetation. Finally, the information available from microwaves is different from that available from visible and infrared frequencies. Therefore, the sensors operating in these three frequency ranges can complement each other. In a similar manner, *active microwave remote sensing* can complement microwave radiometry.

A part of the solar energy incident on the earth gets absorbed, leading to a rise in temperature. Under thermal equilibrium, the absorbed solar radiation is balanced by radiation emitted by the earth's surface and its atmosphere. The energy received by a radiometer is due to radiation, self-emitted and/or reflected (scattered) by the scene, and collected by the antenna. It can be shown that the power P emitted by an object in thermodynamic equilibrium is a function of its physical temperature T, and in the microwave frequency region P is directly proportional to T. The radiometric *brightness temperature* T_{B} is used to characterize the emission by a material, through the expression

$$T_{\mathrm{B}} = \frac{P}{kB} \tag{1}$$

where P is the power emitted by the material over the bandwidth B, and k is Boltzmann's constant. Similarly, corresponding to the power P_{A} received by a radiometer antenna, a radiometric *antenna temperature* T_{A} is defined by

$$T_{\mathrm{A}} = \frac{P_{\mathrm{A}}}{kB} \tag{2}$$

In the general case, T_{A} represents all radiation incident upon the antenna, integrated over all possible directions and weighted according to the antenna directional pattern. In addition, the effects of the atmosphere and self-emission by the antenna structure also have to be considered. These factors are taken into account through the use of radiative transfer theory (5). The scattering effects of geophysical terrain also contribute to microwave measurements. At microwave frequencies, the size of the scatterers and the rough surface heights in a geophysical terrain are comparable to the wavelengths used. Thus, the use of the wave approach based on solutions of Maxwell's equations is essential. This requires a vector radiative transfer formulation (6,7).

The natural radiation emitted and scattered by material media is phase-incoherent and extends over the entire electromagnetic spectrum. Thus, it has a noiselike character. Moreover, the radiometric signal to be measured is much smaller than the noise generated in the receiver. Therefore, radiometers are designed to measure very small signal levels with high precision. Specialized radiometers analyze the received energy's spectral distribution (*spectroradiometers*), its polarization (*polarimeters*), or its angular distribution in space (*imaging radiometers*).

The simplest type of radiometer, called the total or *direct power radiometer*, is shown in Fig. 1. It consists of an antenna, an amplifying predetection stage, a detector, an integrator, and a display section. Since the received signal levels are very low, the predetection stage incorporates a low-noise amplifier and a bandpass filter. This stage utilizes a heterodyne scheme, providing the bulk of amplification at the intermediate frequency (*IF*). For a square-law detector, the output voltage is proportional to the input power. The output voltage consists of a dc component corresponding to the mean input power, and an ac component representing the low-frequency portion of the noise spectrum. The dc component is given by

$$V_{\mathrm{dc}} = G_{\mathrm{S}}\,(T_{\mathrm{A}} + T_{\mathrm{REC}}) \tag{3}$$

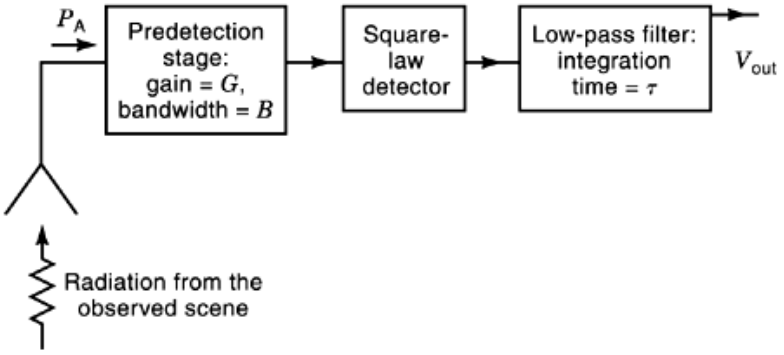

Fig. 1. Block diagram of a total-power radiometer.

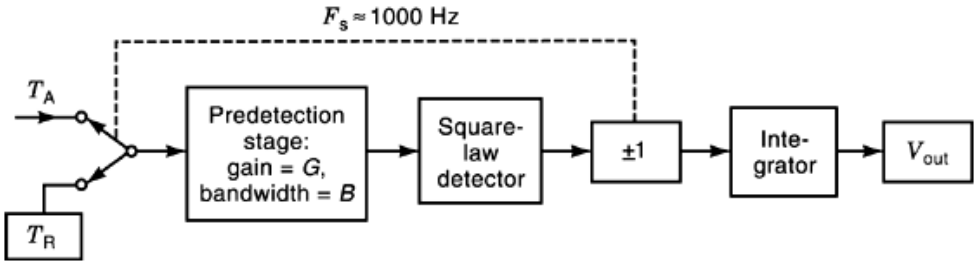

Fig. 2. Block diagram of the Dicke radiometer.

where G_S is the system gain factor and T_{REC} is the equivalent receiver input noise temperature. By calibrating the radiometer using a variable noise source with known noise temperature, the output voltage can be related to the overall noise temperature at the input of the receiver. The resolution in the measurement of the noise temperature is given by

$$\Delta T = \frac{T_A + T_{REC}}{\sqrt{B\tau}} \tag{4}$$

where B is the RF bandwidth of the detected input signal and τ is the integration time. The measurement resolution can be improved by increasing the integration time.

As seen in Eq. (3), in the total power radiometer, output voltage will fluctuate with variations in the receiver gain and noise. In the *Dicke radiometer*, represented in Fig. 2, the receiver input is switched at about 1000 Hz between the antenna temperature and a reference temperature, and the detector output is multiplied by $+1$ or -1, depending on the position of the switch. This eliminates the dependence on receiver noise, since the output voltage is now given by

$$V_{dc} = G_S (T_A - T_R) \tag{5}$$

Figure 3 represents a *noise-injection radiometer*. In this type of radiometer, a servo loop adjusts the temperature T_I of a variable noise generator, which is added to the antenna signal T_A, so that the resultant

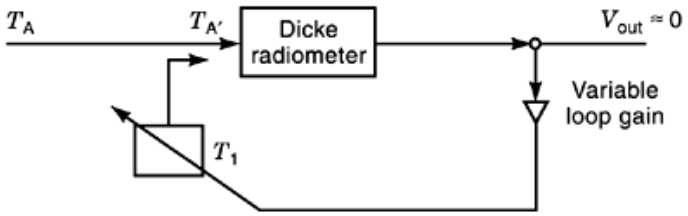

Fig. 3. Block diagram of the noise-injection radiometer.

input $T_{A'}$ to the Dicke radiometer is equal to the reference temperature T_R, and a zero output results. In this case, the output voltage is given by

$$V_{dc} = G_S (T_{A'} - T_R) = 0 \tag{6}$$

and the signal T_A is given by

$$T_A = T_R - T_I \tag{7}$$

Thus, in this type of radiometer, the output is independent of gain and noise-temperature fluctuations.

For applications requiring measurement of the spectral dependence of the microwave emission, a *microwave spectrometer* is obtained by subdividing the passband of the radiometer and separately detecting the output of each segment. More details of the radiometers are available in Refs. 1,8,9.

Applications of microwave radiometry range from astronomical, military, and medical to environmental. Radiometers have been used to measure the radio emission from numerous objects in our galaxy, as well as objects in other galaxies. Atmospheres of a number of planets have been explored using microwave remote sensing. The military use of radiometers is primarily for detecting or locating metal objects; microwave radiometers are used as the prime sensors as a missile approaches a target, since a radiometer emits no warning signal. In clinical medicine, microwave radiometry is used to obtain information about internal body temperature patterns by the measurement of part of the centimetric wavelength component of the natural thermal radiation from the body tissue (10,11). The most extensive application of microwave radiometry has been in geoscientific fields such as atmospheric studies, meteorology, hydrology, agriculture, and oceanography. Microwave radiometry can provide information on atmospheric temperature profile, magnetic-field profile, water-vapor profile, cyclones and storms, soil moisture, floods, snow cover, crop yield, and ocean surface wind, temperature, and oil spills.

Microwave Spectroscopy

Some low-pressure gases absorb electromagnetic radiation in the microwave frequency range. Using a suitable microwave spectrometer, this absorption can be observed as sharp *lines* in the spectrum of an applied microwave swept-frequency signal. Likewise, under thermal equilibrium, the emission from these gases will consist of lines. These lines correspond to the rotational transitions of the gas molecules. A typical frequency range for microwave spectroscopy is 2 GHz to 120 GHz; for specialized applications, the higher frequency may extend up to 500 GHz. This topic has been well covered in a number of books (12,13,14,15,16). Here we provide a simple introduction to the basic considerations and applications of microwave spectroscopy (12).

Through fairly simple considerations, it can be seen that rotational frequency of an ordinary diatomic molecule will be in the microwave frequency range. Assuming that the distance between nuclei in a diatomic molecule is fixed, and that the angular momentum must be some integral multiple of $h/2\pi$, one gets

$$2\pi \upsilon I = \frac{Jh}{2\pi} \tag{8}$$

where h is Planck's constant, I is the angular moment of inertia about the axes perpendicular to the internuclear axis, υ is the frequency of the end-over-end rotation of this rigid rotor, and J is a positive integer. Hence the possible frequencies from such a system are

$$\upsilon = \frac{Jh}{4\pi^2 I} \tag{9}$$

For diatomic molecules of ordinary masses, I is such that for small integral values of J, the frequency υ is of the order of 10 GHz to 100 GHz. Further, the frequency separation $\Delta\upsilon$ can be written as

$$\Delta\upsilon = 2B \tag{10}$$

where B is a molecular constant.

A molecule interacts appreciably with a microwave electromagnetic field to emit or absorb radiation only if it has an electric or magnetic *dipole moment*. Usually, the dipole is an electric moment due to the positive and negative charges in the molecule. At gas pressures near 1 atm (100 kPa), small microwave absorption may occur over a wide frequency range. As the pressure is lowered, the range of frequencies absorbed decreases proportionally down to pressures near 10^{-3} Torr (0.1 Pa), where the range is so small that the term *absorption line* is well merited. Significantly, and contrary to experience in other types of spectroscopy, the intensity of absorption at the center of the line does not appreciably decrease with this enormous decrease in pressure.

The advantages of microwave spectroscopy of gases consist in its high resolution and the use of very low-pressure gases. *Rotational spectral lines*, utilized in microwave spectroscopy, are generally well separated and easily differentiated. On the other hand, in the infrared region, for example, the *rotation–vibration bands* of one substance may become a series of continuous bands and may interfere with the spectra of other substances. In addition to high resolution, only a small quantity of gas is needed. In atmospheric studies using microwave spectroscopy, further advantages of microwave wavelengths are their relative insensitivity to aerosol scattering and to uncertainties in atmospheric temperatures. A microwave spectrometer need not operate over a large frequency range, since most substances have a number of lines throughout the microwave region. Microwave spectroscopy has its limitations too; these arise from the facts that the specimen under study must usually be a dipolar gas, and that the molecules under study should not have a large number of atoms; otherwise the microwave spectra become very complicated.

Compared to Eq. (8), a more rigorous determination of the frequencies produced by a rigid diatomic molecule can be obtained from quantum-mechanical considerations (12). It is very difficult to take into account the entire molecular system, composed of interacting electrons as well as nuclei; however, simplifying approximations are usually possible. Rotational spectra of different types of molecules, such as linear polyatomic, symmetric top, or asymmetric top, have been studied in detail in the literature. Line parameters for a number of gases for selected lines below 300 GHz are available in the literature (16, Appendix to Chap. 2); more complete line-parameter compilations are also available (17).

When spectral lines of atoms are examined closely, they are found to have a *fine structure*. This structure is explained by attributing to the electron a spin angular momentum and a magnetic moment. More careful

observations also reveal a *hyperfine structure* of atomic lines, which results from perturbations of electronic energy levels due to the finite size and mass of nuclei. When an atom is placed in a magnetic field, the energy levels undergo a splitting known as the *Zeeman effect*. Molecular spectra also exhibit similar effects. The origin of the hyperfine structure in molecules is either the nuclear electric quadrupole moment, or, much less commonly, for molecules with electronic angular momentum, the nuclear magnetic dipole moment. Further, the rotational spectrum of a molecule having an electric dipole moment gets modified when the molecule is in an electric field. This is known as *Stark effect*; it provides a means for modulating microwave lines for detection and thus aids in identification of transitions. While typically the Zeeman effect is small in molecules, it may be large for molecules with electronic angular momentum.

Spectral line broadening at microwave frequencies occurs due to two important reasons: *Doppler* (thermal) and *collisional* (pressure). Doppler broadening is described by the Gaussian distribution of kinetic velocities for the absorbing and emitting molecules. The Doppler full width at half maximum ($\Delta\nu_d$) is given by

$$\Delta\nu_d = \frac{\nu}{c}\left(\frac{2kT}{m}\ln 2\right)^{1/2} \tag{11}$$

where m is the molecular mass. For microwave frequencies, at pressures greater than 0.1 mbar (10 Pa), collisional broadening exceeds Doppler broadening. The former has a Lorentzian shape; at low pressures, the collisional line width ($\Delta\nu_c$) is given by

$$\Delta\nu_c = \Delta\nu_{c0}\,(P/P_0)(T/T_0)^{-x} \tag{12}$$

where P and T are the pressure and temperature, and the exponent x is approximately 0.75 for pressures in the range of 0.01 mbar to 1 mbar (1 Pa to 100 Pa). By integrating the absorption coefficient over the frequency range of an absorption line, one obtains the absolute or *integrated line intensity*. Integrated line strengths increase as v^y, with y ranging between 2 and 3, for increasing-order rotational transitions of a given linear molecule. Roughly the same trend holds good for the strongest line transitions for a given nonlinear molecule as well.

The simplified block diagram of a typical conventional microwave spectrometer is shown in Fig. 4. The microwave signal from a swept frequency source is passed through a waveguide or parallel plate cell, 1 m to 4 m long, containing the gas specimen, and the transmission is measured as a function of frequency. *Stark modulation* is achieved by applying a high-voltage square wave at a frequency of about 100 kHz. This modulation reduces the effect of detector and oscillator noise as well as oscillator power variation. A computer can control the oscillator frequency and record the output variation versus frequency. The frequency is accurately measured by comparison with a low-phase-noise synthesizer. The oscillators used are klystrons or backward-wave oscillators. A simple introduction to microwave components and devices, such as waveguides, klystrons, backward-wave oscillators, and detectors, can be found in Ref. 18. In both cases, frequency can be varied electrically—up to 100 MHz for the former, and over a full waveguide band for the latter. The detector is usually a Schottky diode. For very sensitive detectors, a liquid-helium-cooled bolometer may be used.

Higher-resolution spectrometers can be obtained by using the *molecular beam technique*. In this technique, the molecules are confined to a narrow beam by collimating slits; the microwave radiation passes through the beam transversely. Then there are no molecules having more than a small component of velocity in the direction of propagation, and so the linewidth is reduced in proportion to the degree of collimation. Moreover, the gas beam cools as it expands out of the slit. In this manner, Doppler widths can be easily reduced by a factor of 10. Details of such spectrometers are available in Refs. 12 and 15. More recent developments include the pulsed molecular beam Fabry–Perot cavity *Fourier transform microwave spectrometer* (*FTMW*). The FTMW

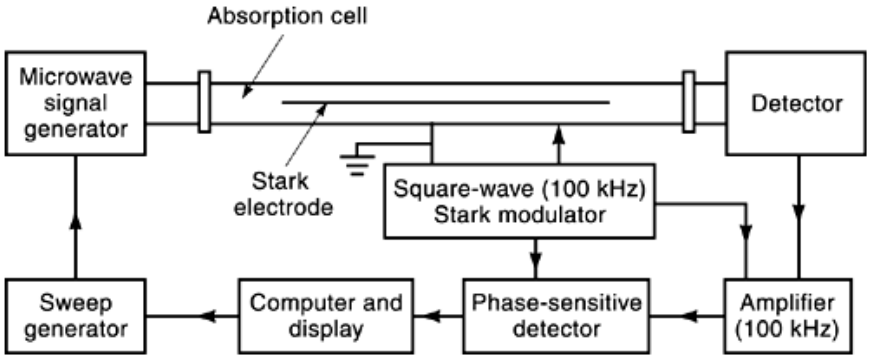

Fig. 4. A microwave spectrometer incorporating Stark modulation.

spectrometer combines molecular beam methods and time-domain Fourier transform spectroscopy, making it a high-resolution and high-sensitivity tool. A description of this instrument is available in Ref. 15.

Microwave spectrometers can be used to identify the contents of a mixture of gases for which microwave spectra are known. It is also possible to measure the fractional abundance of a component of a mixture by measuring the peak absorption coefficient for the corresponding line. Accurate microwave spectroscopic data yield information on moments of inertia, bond distances and bond angles, dipole moments and collision frequencies, nuclear magnetic dipole and quadrupole moments, isotopic masses, and the internal electric fields of molecules. Microwave spectroscopy of the earth's middle atmosphere (stratosphere–mesosphere) has enabled measurements of the rotational transitions for water vapor and a host of gases; most of this information is relevant to ozone photochemistry. Furthermore, ground-based observations allow pressure scale-height resolution of the vertical mixing profile of the measured species (16).

Measurement of Permittivity and Permeability

Analysis and design applications at microwave frequencies often require accurate knowledge of a material's complex *relative permittivity* $\varepsilon_r = \varepsilon'_r - j\varepsilon''_r$ and *permeability* $\mu_r = \mu'_r - j\mu''_r$. These measurements may also be required for purely scientific purposes. A large number of publications describe or review these measurements in detail; see, for instance, Refs. 19,20,21. These references in turn have comprehensive bibliographies. Over the years, almost all methods of measurement of material properties have undergone improvements. Here, the common methods of measurement of complex permittivity and permeability, particularly suitable for the microwave frequency range, will be described briefly, together with some new developments in these methods. The general topics of Dielectric Measurement and Loss-Angle Measurement are described elsewhere also in this encyclopedia.

While the variation of ε'_r with frequency is sufficiently gradual for it to be considered constant over a fairly wide frequency band for most common microwave applications, the percentage variation in ε''_r is always greater than that in ε'_r. Therefore, ε''_r should be measured near the frequency of interest. For many materials, ε_r may depend upon temperature and/or humidity. At microwave frequencies, in addition to permittivity, permeability is also important for magnetic materials such as *ferrites*, which are useful in phase shifters, isolators, circulators, and switches. For ferrites, permeability is a tensor quantity and varies with the biasing dc magnetic field. Unlike pure dielectrics, which generally exhibit only broad relaxations at microwave frequencies, ferrites exhibit sharp ferrimagnetic resonances. In spite of these complications, the methods for the measurement of permeability of ferrites turn out to be similar to those used for pure dielectrics.

The methods included here are based on transmission lines and waveguides; time-domain; closed-cavity, open-cavity, or microstrip resonators; and free-space or free-wave techniques. Each technique has its own advantages and limitations. For measurements over a wide range of frequencies, transmission line or waveguide methods, often incorporating automatic network analyzers (ANAs), are employed. Before the advent of the ANA, time-domain methods, yielding wideband information, were popular. The resonant cavity or cavity perturbation techniques usually offer the highest accuracy, due to the multipass nature of the resonance measurement; however, these are restricted to a narrow frequency band. At the higher end of the microwave frequency range, where it becomes difficult to fabricate high-Q closed cavities, or for high-loss materials for which open resonators are not suitable, one uses free-space or free-wave methods. Like open resonators, these methods also require the material in the form of a big sheet.

Transmission Line and Waveguide Methods. These methods are usually divided into *transmission* and *reflection* methods. The measurements of either the transmission or the reflection coefficient result in transcendental equations linking the measured parameter with permittivity or permeability. The exception is the case when measurements of both s_{11} and s_{12} are attainable. In this case an explicit solution for ε_r and μ_r is obtained as shown in Eqs. (13)–(19)below.

One of the best-known and most widely used reflection method is the *Robert–von Hippel method* (22). In its classical form, the method requires the measurement of location of voltage minima in a short-circuited waveguide with and without a dielectric sample; the complex permittivity is obtained by solving a transcendental equation (20). If the permittivity is not known approximately, two samples of different lengths are used to arrive at a unique solution of the transcendental equation. Improvements to this classical form include use of ANA, computer programs for rapid data reduction, measurements as a function of temperature, and measurements on magnetic materials (21). Another technique is to measure the input impedance of a waveguide containing the specimen, with a short-circuit and an open-circuit termination, respectively, at the far end of the specimen; the complex permittivity is related to the impedances measured in this manner. Simultaneous measurement of permittivity and permeability is also possible using this technique (20). For the case when the material sample has the same cross section as that of the waveguide used for the measurement, the input reflection coefficient is calculated using a simple modal expansion method. When the sample selected is not of uniform cross section or occupies only a part of the waveguide cross section, numerical methods may be required. For such a case, for a rectangular waveguide, a method using the finite-element method is described in Ref. 23.

Measurements of *scattering parameters* on samples placed in a waveguide or transmission line, using ANA, can yield wideband frequency-dependent material properties. Following Ref. 24, for a TEM-mode transmission line, let $s_{11}(\omega)$ and $s_{21}(\omega)$ be the frequency-dependent s parameters for the configuration shown in Fig. 5. Then

$$\mu_r = \sqrt{C_1 C_2}, \tag{13}$$

$$\varepsilon_r = \sqrt{C_1/C_2}, \tag{14}$$

where the parameters C_1 and C_2 are defined completely in terms of $s_{11}(\omega)$ and $s_{21}(\omega)$:

$$C_1 = -\left\{\left(\frac{c_o}{l_2\omega}\right)\ln z\right\}^2 \tag{15}$$

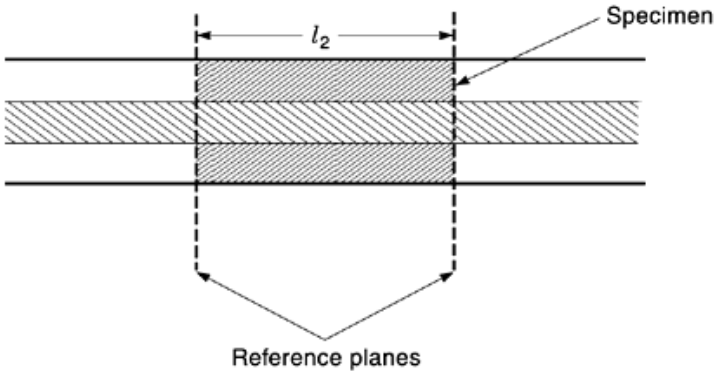

Fig. 5. Coaxial transmission line containing the specimen for which *s*-parameters are measured with reference to the interfaces of the specimen with the rest of the line.

$$C_2 = \left(\frac{1+\Gamma_{12}}{1-\Gamma_{12}}\right)^2 \tag{16}$$

$$z = \frac{s_{11}+s_{21}-\Gamma_{12}}{1-(s_{11}+s_{21})\Gamma_{12}} \tag{17}$$

$$\Gamma_{12} = X \pm \sqrt{X^2-1} \tag{18}$$

$$X = \frac{1-\left(s_{21}^2-s_{11}^2\right)}{2s_{11}} \pm \sqrt{\left[\frac{1-\left(s_{21}^2-s_{11}^2\right)}{2s_{11}}\right]^2-1} \tag{19}$$

c_0 = speed of light in vacuum

Open-ended sensors consisting of waveguide or coaxial transmission lines have proved useful in the measurement of dielectric properties because of their relatively minor constraints on the test material shape and configuration. This method has proved quite convenient for biological and soil samples. The principle of operation of this technique is presented, for instance, in Ref. 25. The sensor is placed in contact with the material under test, and the resulting reflection coefficient is measured using ANA. Knowledge of the relationship between the measured reflection coefficient and the material properties allows one to determine the latter. Because of the open geometry, techniques of computational electromagnetics are required for an accurate analysis. For calibration of the measurement system, *one-port error correction* techniques are utilized. The procedure consists of testing with three standard terminations: an open circuit, a short circuit, and a

liquid with known dielectric properties. The error resulting from the uncertainty in the properties of the known dielectric has been discussed in Ref. 25.

Time-Domain Method. The time-domain technique of measurement of material properties depends on calculating the complex permittivity and permeability from the response of a material specimen to a short-rise-time (tens of picoseconds) pulse. Usually, the time-domain response is transformed to frequency domain and the material properties are estimated over a wide frequency range (e.g., 50 MHz to 8 GHz). The basic technique has been presented in Ref. 26 and reviewed in Ref. 27. An improved data-reduction method is described in Ref. 24 for a coaxial test fixture for determining the frequency-domain s-parameters $s_{11}(\omega)$ and $s_{21}(\omega)$ from the Fourier transforms of the measured reflected and transmitted waveforms. Then one makes use of Eqs. (13)–(19)to calculate the complex permittivity and permeability.

The useful frequency range of the time-domain method increases as the duration of the initial pulse decreases and/or the time resolution of the detection process increases. With recent improvements in optoelectronic techniques using ultrafast lasers, it is now possible to generate subpicosecond electrical pulses. These pulses can be utilized for material characterization up to terahertz frequencies (28). While the basic principle remains as described in the foregoing, some practical details of the technique are described in the section on time-domain measurements in this article.

Cavity Methods. In cavity methods, typically, one measures the resonant frequency f_r and quality factor Q_L for an empty (or air-filled) cavity, as well as for the same cavity perturbed by a small specimen of the material under investigation. In such a case, the perturbation equation gives the following approximate relations (29):

$$\frac{\omega_2 - \omega_1}{\omega_2} \approx \frac{(\mu - \mu_0) \int_{V_s} \boldsymbol{H}_1 \cdot \boldsymbol{H}_2 \, dV - (\varepsilon - \varepsilon_0) \int_{V_s} \boldsymbol{E}_1 \cdot \boldsymbol{E}_2 \, dV}{2\varepsilon_0 \int_{V_c} |\boldsymbol{E}_1|^2 \, dV} \tag{20}$$

$$= \frac{f_{r2} - f_{r1}}{f_{r2}} + \frac{j}{2}\left(\frac{1}{Q_{L2}} - \frac{1}{Q_{L1}}\right) \tag{21}$$

where μ and ε are the material properties, subscripts 1 and 2 refer to the empty and the perturbed cavity, V_s is the sample volume and V_c the cavity volume, and Q_L takes into account all cavity losses. For a nonmagnetic material, the first term in the numerator in Eq. (20) drops out. For a magnetic material, one first determines the permittivity by placing the specimen in the cavity in a region where H is practically zero. Next, the permeability is determined in a similar manner.

The perturbation formulas (20) and (22) give only approximate solutions for permittivity and permeability. More accurate methods require solving a full electromagnetic problem for a sample located inside a resonator. To simplify this problem, usually a circular cylindrical sample is considered. Numerical techniques such as the method of moments or the finite-element method are used to handle this problem.

Simple specimen geometries, such as rods or spheres, are preferred to keep the mathematics simple; the major axis of the specimen is kept either parallel or perpendicular to the field in the cavity. Measurement errors for different sample shapes for a pillbox cavity have been considered in Ref. 30. Cavity methods require stable sources and accurate frequency measurement. One may use the cavity in either transmission mode or reflection mode. In place of frequency variation, cavity length variation can also be made use of. For a low-loss material, one may require larger samples in the cavities. The cases in which the cavity may be completely or partially filled with the specimen have been described in detail in Ref. 20. In addition to using waveguide

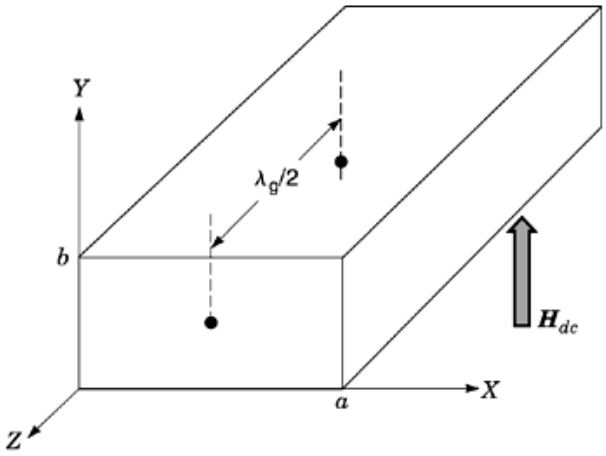

Fig. 6. TE_{102}-mode rectangular cavity. Black dots indicate the locations suitable for placing the sample. At these locations h_x is maximum.

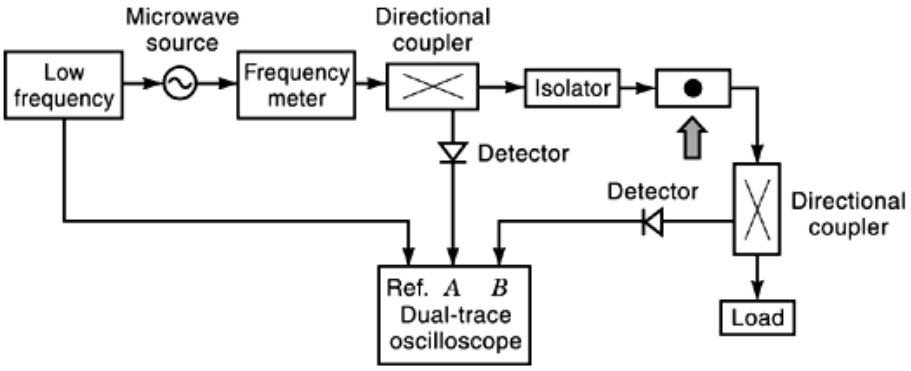

Fig. 7. Measurement setup for properties of ferrites.

cavities, one may also use *microstrip resonators*; this alternative is quite suitable for measurement of the properties of microstrip substrates (31).

For *ferrites*, at microwave frequencies the permeability varies with the applied dc magnetic field and is a tensor, which means that the magnetic flux density and magnetic field are not parallel:

$$\boldsymbol{\mu} = \begin{bmatrix} \mu^* & -j\kappa^* & 0 \\ j\kappa^* & \mu^* & 0 \\ 0 & 0 & 1 \end{bmatrix} \tag{22}$$

By an appropriate choice of the geometry of the microwave and static magnetic fields, the changes in frequency and quality factor of the cavity can be written in terms of the scalar elements of the permeability tensor (32). Figure 6 illustrates the use of a TE_{102} rectangular transmission cavity for this purpose. The measurement setup is shown in Fig. 7.

At higher microwave frequencies (20 GHz to 30 GHz or higher), it becomes difficult to construct precision specimens and high-Q dominant-mode cavities. In such a case, it is possible to use oversize cavities (33), but even at millimeter wavelengths these are rather large. An attractive alternative is to use *open resonators*, which offer very high Q's. An open resonator is a quasioptical analog of the Fabry–Perot resonator and can offer high quality factors, for example, in excess of 10^5 at 35 GHz; therefore, very accurate measurements can be made. The material, in the form of a thin sheet, is inserted between the mirrors constituting the open resonator. The mirrors are spherical in shape. Once again, the material properties are related to the resonant frequency and quality factor of the empty and the perturbed resonator. Design of open resonators and their application in measurement of complex permittivity has been reviewed in Ref. 34. Open resonators are commonly used for the measurement of low-loss materials in the frequency range 30 GHz to 200 GHz. Their high Q can be exploited at lower frequencies as well, but the required specimen size becomes large. The high Q also calls for care in measurements. However, with computer-controlled synthesized signal sources and microwave receivers, an automated measurement system for data collection and processing can usually be configured (35). An automated cavity-length variation system for measurement of complex permittivity is described in Ref. 36.

Free-Space Method. For high-loss materials at high frequencies, resonant methods fail, and it becomes difficult to machine a specimen to fit in a waveguide. In such a case, free-space, or *free-wave*, methods become especially suitable (37,38). Simultaneous determination of complex permittivity and complex permeability can be carried out by using a beam of electromagnetic radiation and measuring the reflection and/or transmission coefficients of planar samples, at normal or oblique incidence (39). The *Fresnel's equations* for a plane wave incident on a plane interface are

$$\begin{aligned} \Gamma_{\parallel} &= \frac{\left(\mu_r\varepsilon_r - \sin^2\theta\right)^{1/2} - \varepsilon_r\cos\theta}{\left(\mu_r\varepsilon_r - \sin^2\theta\right)^{1/2} + \varepsilon_r\cos\theta} \\ \Gamma_{\perp} &= \frac{\mu_r\cos\theta - \left(\mu_r\varepsilon_r - \sin^2\theta\right)^{1/2}}{\mu_r\cos\theta + \left(\mu_r\varepsilon_r - \sin^2\theta\right)^{1/2}} \end{aligned} \tag{23}$$

where θ is the angle of incidence. Taking into account the multiple reflections within the sample, the total reflection (R) and transmission (T) coefficients are given as

$$\begin{aligned} R &= \frac{\left(1-P^2\right)\Gamma}{1-\Gamma^2P^2} \\ T &= \frac{\left(1-\Gamma^2\right)P}{1-\Gamma^2P^2} \end{aligned} \tag{24}$$

where P is the complex propagation factor through the sample and is given by

$$P = \exp\left\{\frac{-j2\pi d}{\lambda_0}\left(\mu_r\varepsilon_r - \sin^2\theta\right)^{1/2}\right\} \tag{25}$$

Here λ_0 is the free-space wavelength and d is the thickness of the sample. The measurements of amplitude and phase of oblique reflection from the sample at two different polarizations of the incident wave result in

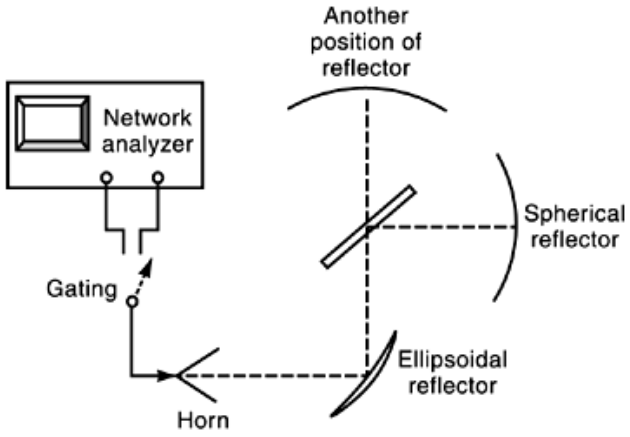

Fig. 8. Free-space measurement of permittivity and permeability.

four sets of data. Manipulating the above equations, one gets

$$\begin{aligned} \varepsilon_r \mu_r &= \frac{\sin^2\theta}{1-\left(\frac{1-\Gamma_\perp}{1+\Gamma_\perp}\right)\left(\frac{1+\Gamma_{||}}{1-\Gamma_{||}}\right)\cos^2\theta} \\ \frac{\varepsilon_r}{\mu_r} &= \left(\frac{1-\Gamma_\perp}{1+\Gamma_\perp}\right)\left(\frac{1-\Gamma_{||}}{1+\Gamma_{||}}\right) \end{aligned} \tag{26}$$

If the measurements are made at several frequencies, one gets a better estimate of the permittivity and permeability. Carrying out this experiment over a certain frequency range, the *dispersion* of material constants can be estimated.

An experimental setup for this measurement is shown in Fig. 8. In this kind of double-pass measurement, both transmission and reflection from the sample can be measured by moving the spherical reflector from one position to the other. Using a simple pyramidal horn (other types of horns also can be used), the wave can be beamed as well as received. The reflected signal can be separated from the transmitted one by the time-domain gating feature of the network analyzer. This method gives results with an accuracy of $\pm 5\%$ when the samples are thin (thickness $\leq \lambda/3$).

Time-Domain Measurements

Time-domain measurement is a method in which the physical quantities of interest, such as voltage or current, are dealt with in their time-dependent form. There are very wideband networks, such as a TEM line, that are represented conveniently in time domain as opposed to frequency domain; the impulse response in such cases is just a delayed impulse. For practical purposes, an impulse is approximated by a short pulse whose duration is much shorter than the duration of the impulse response. Frequently, work with microwave networks is carried out in the frequency domain because of its mathematical convenience. However, in many situations, time-domain measurements offer clear insight, simplicity of concept, and results that perhaps cannot be obtained using frequency-domain techniques. Furthermore, designers of digital circuits prefer to work in the

time domain with logic analyzers and high-speed oscilloscopes. Time-domain measurements in the field of electromagnetics have been reviewed in Ref. 40, which contains comprehensive, state-of-the-art description (at the time of its publication) of various aspects of time-domain measurements. In this section, we briefly mention the advantages, the principles, and some of the major applications of time-domain measurements. Recent developments in optoelectronic techniques, enabling one to produce subpicosecond pulses, have greatly extended the frequency range of these techniques (41,42); examples in this category will also be briefly described.

Some of the advantages of time-domain measurements are (40, Appendix):

(1) Equipment faults, and such as poor connections, cable faults, and impedance mismatches, are easily located in the time domain.
(2) The time domain offers a natural representation of transient-wave phenomena, affording an intuitive understanding of the physics of propagation.
(3) Broadband measurements can be carried out without swept-frequency apparatus.
(4) Time-range gating can be used to suppress reflections from discontinuities or surroundings. This eliminates the need for expensive anechoic chambers.
(5) Usable time-domain data can be obtained without precision calibration standards or techniques. Such standards and techniques are unavoidable in frequency-domain measurements, and automated procedures are commonly required for this purpose.
(6) The time domain is natural for applications such as electromagnetic pulse (EMP) and range-delay radar.

Time-domain measurements have certain limitations too. The most important among these are the unavailability of specialized time-domain equipment in many laboratories, and the measurements usually being limited to frequencies below about 10 GHz. However, as mentioned earlier, with advances in techniques, a number of research groups have demonstrated that the upper frequency for such measurements can be extended to the terahertz range.

The time-domain techniques have been applied to a number of different types of measurements. These include time-domain reflectometry (*TDR*), measurement of material properties, radiation properties of antennas, EMP measurements, target-signature analysis, characterization of monolithic microwave and millimeter-wave integrated circuits (*MMICs*), and characterization of transmission lines and waveguides. Here, we include brief descriptions of TDR and the use of optoelectronic techniques for characterization of materials, transmission lines, and MMICs. A detailed description of TDR is included elsewhere in this encyclopedia (see Reflectometers, Time-domain). Use of conventional short electrical pulses for time-domain material characterization has been briefly described in the section on Measurement of Permittivity and Permeability in this article.

Time-Domain Reflectometry (43,44). In its most popular form, TDR involves generation of a fast steplike signal, which is launched into the transmission line, cable, or circuit under investigation. Using a fast oscilloscope, the incident and reflected voltage waves are monitored at a particular point in the circuit. From these observations, it is possible to locate multiple discontinuities and mismatches, determine the nature of termination, and evaluate cable loss. The common scheme for TDR is shown in Fig. 9, and an idealized response for a resistive termination is shown in Fig. 10. It is assumed that the step generator's impedance matches the characteristic impedance of the cable or device connected to the generator and that the transmission line is lossless. The location D of a discontinuity or mismatch is given by

$$D = 0.5 v_d t_d \tag{27}$$

where v_d is the velocity of the wave on the transmission line and t_d is the two-way transit time, from monitoring point to the mismatch and back again, as measured on the oscilloscope. The value of the reflected wave voltage

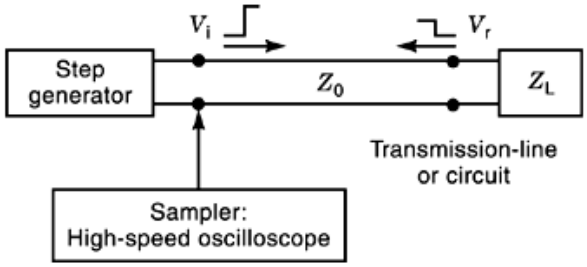

Fig. 9. Basic scheme used in time-domain reflectometry.

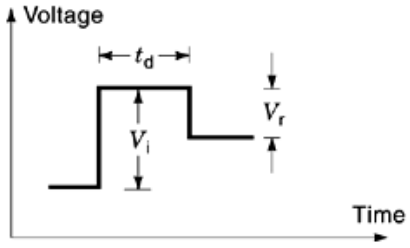

Fig. 10. Idealized response for a resistive termination.

is given by

$$\frac{V_r}{V_i} = \frac{Z_L - Z_0}{Z_L + Z_0} \tag{28}$$

where Z_0 is the characteristic impedance of the transmission line and Z_L is the load impedance. For multiple discontinuities, there occur multiple reflected waves, each of which is seen on the oscilloscope as a distinct step; the height of each step is governed by the corresponding reflection coefficient. For terminations with complex impedance, the reflected wave is more complicated than a simple step. For instance, for an inductive load, the reflected wave is a positive step followed by an exponential decay. Detailed response for such cases are available in Refs. 43,45, and 46.

Time-domain reflectometry can also give information on transmission line losses. For a line in which series losses dominate, the sampled voltage shows an exponentially rising characteristic, while those in which shunt losses dominate show an exponentially decaying characteristic.

Similar results to those described above can be obtained by using a narrow pulse instead of a steplike signal. High resolution in time is achieved by applying very short pulses with durations of a few nanoseconds. This type of reflectometry is very popular for testing long-distance cables, including optical fibers. In such a system, the incident and reflected pulses superimpose when they are close to each other. However, signal processing in the reflectometer can still separate the two waves and determine the required parameters.

Time-Domain Measurements Using Optoelectronic Techniques for Broadband Characterization. In the time-domain measurement technique, a narrow pulse is generated and launched onto the material or transmission line under study. After propagation through the test specimen, the pulse is detected. Through Fourier analysis of the input and propagated pulses, the frequency-dependent absorption and dispersion of the specimen can be obtained. This method, as applied to measurement of material properties, has been described in the section on measurement of permittivity and permeability. Typically, when conventional electronic means

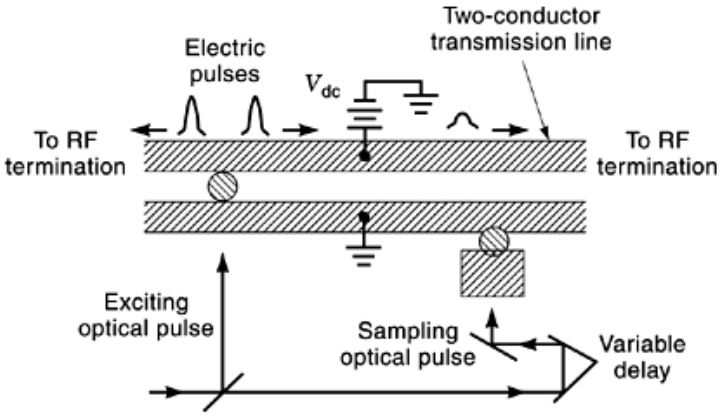

Fig. 11. Schematic diagram of electric pulse generation and detection.

are used for generation of the pulse, the upper frequency limit is around 10 GHz. However, when one uses optoelectronic means for generation of the pulse (41), pulse widths can go down to subpicosecond level. The corresponding frequency range of measurements therefore extends to terahertz range. For the detection of such narrow pulses, once again optoelectronic techniques are used. Frequently, this method of characterization of materials and transmission lines is called *terahertz time-domain spectroscopy* (47,48); when this method is applied to on-wafer characterization of MMICs, it has been referred to as the *ultrafast* or *picosecond optoelectronic technique* (41,49).

The generation and detection of ultrashort electric pulses using optoelectronic techniques is shown schematically in Fig. 11. A two-conductor transmission line, such as a coplanar transmission line, is printed on a semiconducting substrate. A bias voltage is applied between the two conductors. When the gap between the two conductors is illuminated by a focused laser beam at a suitable wavelength, electron–hole plasma is generated at the illumination spot. With sufficient optical energy, the two conductors are short-circuited, leading to flow of current. A high optical energy density is achieved by combining high laser power with a narrow gap between the conductors. When the excitation optical beam is switched off, the current flow stops in a time that depends on the lifetime of the photogenerated carriers. A short carrier lifetime (tens of femtoseconds) is ensured by oxygen or proton implantation. The laser pulse width can be as small as 70 fs, with a repetition rate of about 100 MHz. This transient shorting of the line produces a short electric pulse, which divides into two halves, traveling in opposite directions on the line. One of these is absorbed in a matched load, while the other one propagates through the test structure. For broadband characterization, excitation and propagation in a single mode is a key issue.

As the propagating pulse travels along the line, a voltage appears across the gap between the two conductors. For detection of the propagating pulse, one may use either electro-optic (*EO*) or photoconductive (*PC*) sampling. The latter has been shown to be far more sensitive. In PC sampling, at the sampling location, a secondary gap is short-circuited by a sampling laser pulse. This causes a small amount of current to flow during the time of short circuit, the amount of collected charge being proportional to the voltage across the gap during the sampling interval. The collected charge is measured versus the relative time delay between the excitation and sampling pulses. The collected charge represents a time convolution of the sampling pulse and the detected pulse. The sampling pulse is obtained from the excitation pulse itself, using a beamsplitter. The part of the pulse that is used for sampling is passed through a computer-controlled variable delay line, which can provide delays of up to about 1 ns. The detection process is carried out at two places: one is very close to the excitation point [this gives the characteristics of the input pulse, say $E_i(t)$]; the other is near the output of

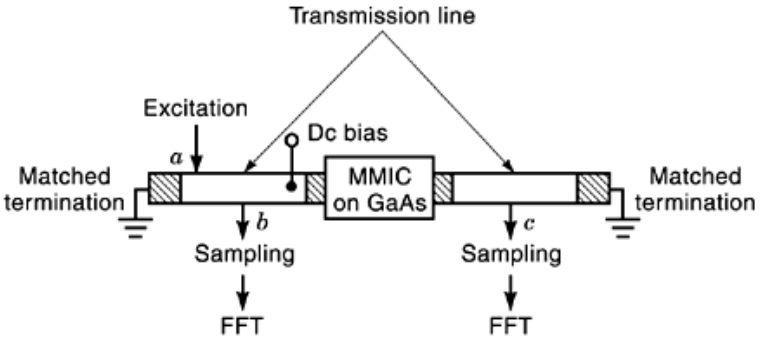

Fig. 12. Schematic of the two-port S-parameter measurement system.

the test specimen [this gives the characteristics of the output pulse, say $E_o(t)$]. By using an appropriate time window for sampling, the measured response can be made to correspond to either the transmitted wave or the reflected wave.

The measured pulse responses are transformed to frequency domain for determining the characteristics of the specimen under test. For example, supposing that the specimen is a transmission line, the spectral component at frequency ω of the transmitted pulse $E_o(\omega)$ is related to the attenuation coefficient α and the phase constant β as follows:

$$E_o(\omega) = E_i(\omega) \exp(j\beta z) \exp(-\alpha z) \tag{29}$$

where z is the propagation distance. Thus one can determine α and β as functions of frequency over a very broad range of frequencies. In this manner, coplanar transmission lines, metal waveguides, and dielectric waveguides have been characterized up to about 1 THz (48).

The technique described above has also been shown to be useful for broadband on-wafer testing of MMICs (42,49). The schematic of such a system is shown in Fig. 12. Let the frequency domain spectra of the various measured voltages are described as follows:

$E_{bi}(\omega)$: Incident voltage at b (port 1)
$E_{br}(\omega)$: Reflected voltage at b (port 1)
$E_{ci}(\omega)$: Transmitted voltage at c (port 2)
$E_{cr}(\omega)$: Reflected voltage at c (port 2)

Then

$$S_{11}(\omega) = \frac{E_{br}(\omega)}{E_{bi}(\omega)} \tag{30}$$

$$S_{21}(\omega) = \frac{E_{ci}(\omega)}{E_{bi}(\omega)} \tag{31}$$

The complex scattering parameters $S_{12}(\omega)$ and $S_{22}(\omega)$ can also be obtained in a similar manner, by arranging excitation at port 2 instead of port 1.

The above technique requires only dc excitation of the circuit under test. It does not require launching or collection of a microwave or millimeter-wave test signal, which usually calls for expensive coplanar waveguide (*CPW*) probes, which suffer from wear and tear due to the mechanical contact. The photoconductive switch can be fabricated on wafer using process steps similar to those used in GaAs MMICs. Moreover, the frequency range of characterization can extend from dc to about 1 THz.

Sweep Frequency Measurement of Scattering Parameters

In most RF and microwave systems, the scattering-parameter (*S*-parameter) representation plays a central role. This importance is derived from the fact that practical system characterization can no longer be accomplished through simple open- or short-circuit measurements. The generalized *n*-port scattering representation is given by (50,51)

$$S = \begin{bmatrix} S_{11} & S_{12} & \cdots & S_{1n} \\ S_{21} & S_{22} & \cdots & S_{2n} \\ \vdots & \vdots & & \vdots \\ S_{n1} & S_{n2} & \cdots & S_{nn} \end{bmatrix} \tag{32}$$

The parameter S_{ii} is the reflection coefficient at the ith port when all other ports are match-terminated. The parameter S_{ij} is the transmission coefficient for waves traveling from the jth port to the ith port when all other ports are match-terminated. With the *S*-parameters, the RF engineer has a tool to characterize multiport networks.

Quite often two-port network measurements are done. In a two-port network, the normalized incident and reflected waves can be expressed by

$$a_n = \frac{V_n - V_{rn}}{\sqrt{Z_0}} \tag{33}$$

$$b_n = \frac{V_n - V_{in}}{\sqrt{Z_0}} \tag{34}$$

where the a's represent normalized incident waves and the b's represent normalized reflected waves at the corresponding ports. The total voltage wave is the sum of incident and reflected voltage waves V_{i} and V_{r}, respectively:

$$\begin{aligned} V_1 &= V_{\mathrm{i}1} + V_{\mathrm{r}1} \\ V_2 &= V_{\mathrm{i}2} + V_{\mathrm{r}2} \end{aligned} \tag{35}$$

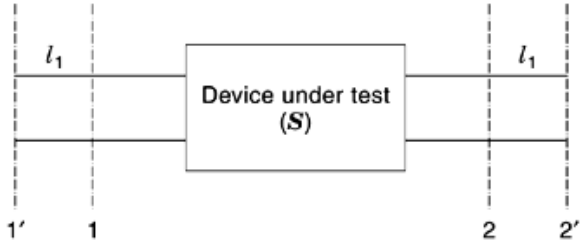

Fig. 13. Complex S-parameter measurements with reference planes.

In the normalization process, the characteristic impedance is normalized to unity, and for a two-port network the relation between incident and reflected waves in terms of scattering parameters is given by

$$\begin{bmatrix} b_1 \\ b_2 \end{bmatrix} = \begin{bmatrix} S_{11} & S_{12} \\ S_{21} & S_{22} \end{bmatrix} \begin{bmatrix} a_1 \\ a_2 \end{bmatrix} \tag{36}$$

where $S_{11} = b_1/a_1|_{a2=0}$, $S_{22} = b_2/a_2|_{a1=0}$, $S_{12} = b_1/a_2|_{a1=0}$, $S_{21} = b_2/a_1|_{a2=0}$. In general the scattering parameters are complex quantities and are defined with respect to the positions of the port or reference planes. For a two-port with unprimed reference planes as shown in Fig. 13, the S-parameters have definite complex values in Eq. (36). If the reference planes 1 and 2 are shifted outward to 1′ and 2′ by electrical phase shifts, the additional lengths have to be taken into account.

Measurement of the S-parameters of a two-port network requires reflection and transmission evaluations of traveling waves at both ports. One of the most popular methods is to use a vector network analyzer. The vector network analyzer is an instrument that can measure RF voltages in terms of magnitude and phase. More details on the internal system blocks and the operation of network analyzers can be found elsewhere (52,53).

Usually network analyzers have one output port, which provides the RF signal either from an internal source or from an external signal generator, and three measurement channels, which are denoted as R, A, and B (refer to Fig. 14). The RF source is typically set to sweep over a specified frequency range. In earlier types of vector network analyzers a voltage-controlled oscillator was used to tune the frequency. In modern types frequency synthesizers are used to achieve this task. The measurement channel R is employed for measuring the incident wave. Channel R also serves as a reference port. Channels A and B usually measure the reflected and transmitted waves, respectively. In general, the measurement channels A and B can be configured to record any two parameters with a single measurement setup. The magnitude and phase of S_{11} can be obtained by evaluating the ratio A/R, and S_{21} by computing B/R. To measure S_{12} and S_{22}, one has to reverse the device under test.

In a realistic measurement system neither the matching conditions nor the ideality of the components is guaranteed. So, to eliminate the effect of all undesired influences such as mismatches or parasitics associated with the input and output ports of the test device, appropriate calibration has to be performed. The network analyzer treats everything between the measurement reference planes as a single device. The primary reference plane for measurements of complex voltages, which are then converted into S-parameters, is usually somewhere inside the network analyzer. This can be achieved by using appropriate calibration standards (54,55) (refer to Standing Wave Meters and Network Analyzers for more details on error models and correction terms).

Until the late 1970s, only discrete frequency measurements were available for characterization of RF and microwave components. Sweep frequency measurements give the benefits of speed, convenience, and the ability to display measurement results instantaneously over the frequency range of interest. These sweep

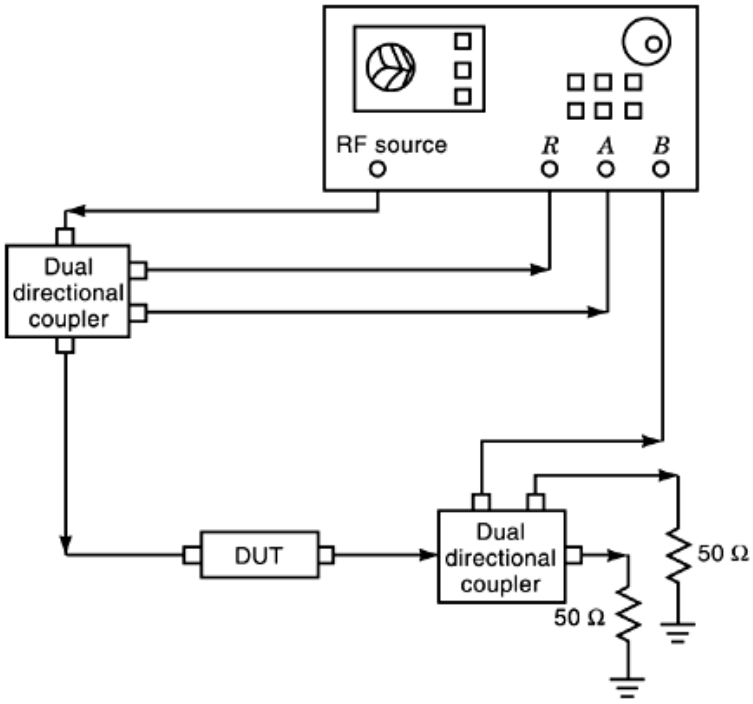

Fig. 14. Measurement system for S-parameters using a network analyzer.

measurements are important in characterizing and understanding the properties of components used in broadband systems. Sweep frequency measurements became popular with the advent of backward-wave oscillators. For many years, swept-frequency oscillators, or sweepers, were manufactured on a modular basis. More recently, sweepers have become available that cover the entire range from 10 MHz to 40 GHz without the need to change the plug-ins, a development that has been associated with the introduction of a K-type coaxial connector, which does not overmode at frequencies up to 45 GHz (56). More details on swept-frequency systems, ranging from the most sophisticated vector automatic network analyzers to simple frequency-response test-set plug-ins, are available in the published literature and application notes from manufacturers.

One of the most important considerations in sweep measurements is constant output power. For example, this becomes very important while testing nonlinear devices, because their performance depends on the level of the incident signal. The power output from a sweep oscillator can vary greatly across a band, which is inconvenient for measurements, since it may be impossible to distinguish the properties of the test device from those of the swept source. The technique of automatic level control is used to overcome this problem by reducing peak powers to the same level as the minimum power available in the band. Also, great care should be taken to ensure that spurious signals from the synthesizer do not affect measurements (57).

The sweep measurement can also be employed to estimate the quality factor of the cavity by observing the transmission coefficient's response over a narrow frequency range of interest. By measuring S_{21} over a narrow frequency range, reading the resonant frequency and 3-dB-down bandwidth, the quality factor of a cavity can be estimated. Sweep measurements can also be useful in characterizing the microwave substrate materials and in the design of active circuits used at RF and microwave frequencies (58,59,60).

Six-Port Reflectometer

The determination of scattering parameters of microwave devices has been largely done by the well-known heterodyne network analyzer. It can provide fast and accurate measurements up to the millimeter wave range. However, because of its high cost, a new technique, introduced by Glenn Engen and Cletus Hoer, the six-port technique (61,62,63,64), has been gradually drawing the attention of metrologists and industry. The six-port reflectometer is a measurement device that is mainly used in high-frequency electronics. It allows one to measure both the amplitude ratio and the phase difference of two electromagnetic waves. The most frequent use of this device is for measuring the so-called complex reflection coefficient (Γ_1) of a device under test (*DUT*), which is the ratio of the amplitude of the wave reflected by the DUT to that of the wave incident on the DUT. The reflection coefficient is directly related to the input impedance of the DUT. It can lead to the determination of the scattering parameters of microwave devices from power measurements only, without the complex circuitry of the heterodyne network analyzer (65,66).

Normally, a six-port reflectometer can produce a set of four power readings. One of these readings is used as a reference, while the rest can be modified to produce three circles in the complex plane in order to determine the reflection coefficient. These circles are supposed to intersect at a single point, which represents Γ_1. The six-port technique consists in determining the complex reflection coefficient from the intersection of the three circles in the complex plane, whose centers and radii depend on the characteristics of hardware employed and the powers collected at specific ports of the equipment. This six-port network analyzer can operate as a reflectometer, measuring only the reflection coefficients, or as a complete system, which also measures the transmission coefficients (67). A six-port reflectometer is in principle simply a passive linear circuit with two input ports and four output ports (hence its name), which provides at its outputs four different linear combinations of the waves present at its inputs.

Figure 15 shows the six-port reflectometer used to provide the complex ratio a_2/a_1 of the two incident microwave signals at ports 1 and 2. Ports 3 to 6 are connected to four detectors. If the six-port junction is linear, its behavior can be described by a scattering matrix S, which relates the reflected power waves b_i and the incident power waves a_i:

$$b_i = \sum_{j=1}^{6} S_{ij} a_j, \qquad i = 1, \ldots, 6 \tag{37}$$

while the boundary conditions imposed by the detectors are

$$a_j = \Gamma_j b_j, \qquad j = 3, \ldots, 6 \tag{38}$$

where Γ_j is the reflection coefficient of the jth detector.

Equations (6.1) and (6.2) yield

$$b_j = A_j a_1 + B_j a_2, \qquad j = 3, \ldots, 6 \tag{39}$$

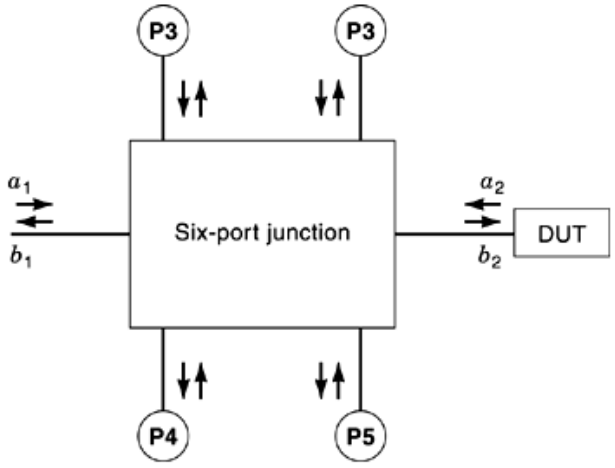

Fig. 15. The six-port reflectometer.

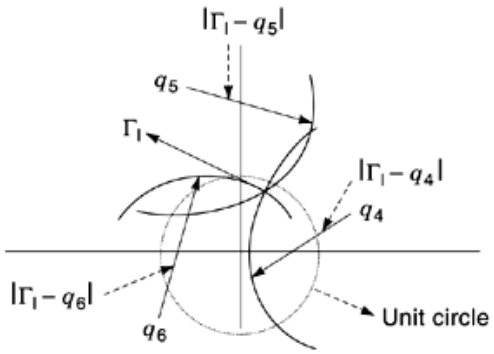

Fig. 16. Determination of reflection coefficient from the intersection of three circles in the complex Γ_l plane.

where A_j and B_j are functions of the scattering parameters of the six-port junction and the reflection coefficients of the detectors. The six-port equations can be written as

$$\frac{P_i}{P_3} = k_i \left| \frac{\frac{a_2}{a_1} - q_i}{\frac{a_2}{a_1} - q_3} \right|^2, \qquad i = 4, \ldots, 6 \tag{40}$$

where $k_i = |B_i/B_3|$ and $q_i = -A_i/B_i$ are known real and complex parameters, respectively. Thus the unknown a_2/a_1 can be determined in magnitude and phase by three power-meter readings normalized to the fourth, which should measure the incident power level. The above equations are complex bilinear transformations, which also transform circles into circles in the complex plane. The centers of these circles are the points q_i, and their radii are proportional to the ratios P_i/P_3 of the powers measured by the detectors (68,69,70,71). Figure 16 represents determination of Γ_l from the intersection of the circles of the measured values. In practice, because of measurement errors, the three circles will not intersect in a point, and some sort of statistical weighting is called for.

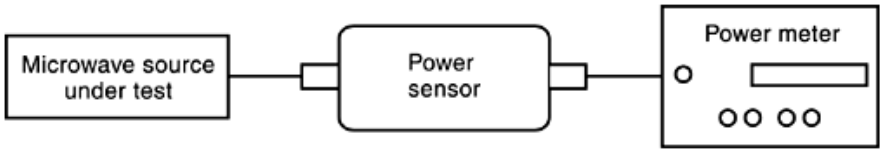

Fig. 17. Power measurement setup.

In the standard application, six-port reflectometers are used to perform reflection coefficient measurements on a given load. To extend the six-port techniques to measuring a full set of scattering parameters, a single six-port reflectometer with a suitable switching system can be used (68,72). An alternative solution for the same purpose is to use a dual six-port system (65,73).

An indirect measurement technique like this requires both careful calibration of the measurement system (the six-port reflectometer) and a rather sophisticated mathematical procedure to obtain the quantity of interest (the complex reflection coefficient) from the raw measured data (the four amplitudes at the output ports). Prior to calibrating the six-port, its power detectors need to be calibrated. The difficulty in calibrating the detectors depends on the type of the detectors used in the system. Linear detectors such as thermistors do not need to be calibrated. However, they are inconvenient in their large power requirement and their slow response. Semiconductor detectors such as Schottky barrier detectors are more sensitive and have a faster response. However, due to their nonlinear behavior, they require precise calibration. This calibration can be avoided by using special measurement arrangements (74).

Power Measurement

The measurement of microwave power is important for design and testing engineers to characterize materials or microwave devices used in a variety of applications. Power is defined as the quantity of energy dissipated or stored per unit time. The range of microwave power is divided into three categories—low power (<10 mW), medium power (10 mW to 10 W), and high power (>10 W).

The microwave power meter consists of a power sensor, which converts microwave power into heat energy, and the final power indication is obtained directly or indirectly by measuring the temperature rise of the power-sensitive element (75,76,77,78). The most important consideration in using such thermal devices is linearity between temperature rise and the impressed power. The measurement setup is shown in Fig. 17.

Thermally sensitive power sensors may be classified into two types: bolometric calorimetric. *Bolometer* is a generic term for any device that changes its electrical resistance with power absorption. A *calorimetric* power sensor is one whose heat absorption is measured by a temperature-sensitive indicator external to the thermal element itself. High power is often measured, especially for standards and calibration purposes, using a microwave calorimeter in which the temperature rise of the load provides a direct measure of the power absorbed by the load.

Bolometric Methods. The two most common types of bolometer are the baretter and the thermistor. The *baretter* is a thin metallic (platinum) wire with a positive temperature coefficient of resistance. A *thermistor* is a semiconducting material with negative temperature coefficient of resistance, and can be easily mounted in microwave transmission lines or waveguides. Baretters are more delicate than thermistors and due to this mechanical fragility they are used only for very low power (up to a few milliwatts). Medium and high power levels are measured with a low-power thermistor sensor with proper attenuators.

Double-balanced-bridge power measurement is shown in Fig. 18. The upper bridge circuit measures the microwave power, and the lower bridge circuit compensates the effect of ambient temperature variation. The microwave power impressed on the arms of the bridge will alter the bolometer's resistance, causing an

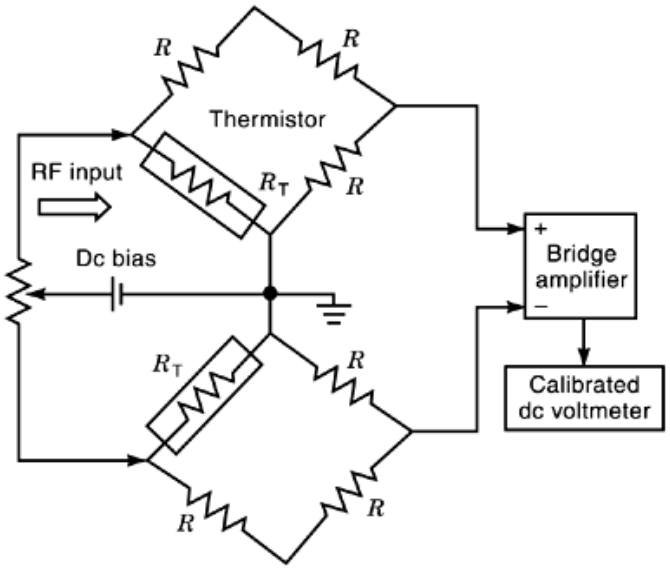

Fig. 18. Double-balanced-bridge measurement of power.

imbalance from its initial balanced condition, which is achieved under zero incident power. The nonzero output is recorded on a voltmeter, which is calibrated to read the input microwave power. The mismatch due to the impressed power is compensated through a self-biasing circuit by decreasing the dc power carried by the RF sensing thermistor until bridge balance is restored (79,80,81,82).

A *thermocouple* is a junction of two wires of different metals or semiconductors. It generates a proportional voltage when the two ends are heated up differently. By appropriate calibration the temperature is converted into the power to be measured. A power sensor using a thermocouple and its associated circuit is shown in Fig. 19. The capacitor C_1 is a dc block, and C_2 is an RF bypass capacitor. The potentials created in the parallel thermocouples are added and will appear across C_2. The dc voltmeter reads a voltage proportional to the input microwave power. Thermocouples have high sensitivity and are used in low- and medium-power measurements (83).

Calorimetric Method. This is the most fundamental method of measuring microwave power. Calorimetric power meters are categorized into flow (liquid) and static (dry) (84,85). The flow-type calorimeter uses a liquid to carry the heat away from the load in a controlled manner. The dissipation of power in the load is measured by letting cooling liquid flow in or around the load and measuring its temperature rise. The basic measurement setup for a flow-type microwave calorimeter is shown in Fig. 20. The static calorimeter measures the electromagnetic field generated in a thermopile placed between a reference level and an active one dissipating input power. The disadvantage of calorimeter measurement is the thermal inertia caused by the lag between the application of microwave power and the parameter readings.

The errors normally encountered in microwave power measurements are due to mismatch loss, RF loss, and substitution error. The mismatch loss can be reduced by inserting attenuation to reduce the reflections and present a good match to both the load and the source. The RF loss and substitution error are regarded as a single factor associated with the calibration factor. By using a thermistor with a calibration figure of about 0.9 to 1, one can compensate for errors in the overall power measuring system.

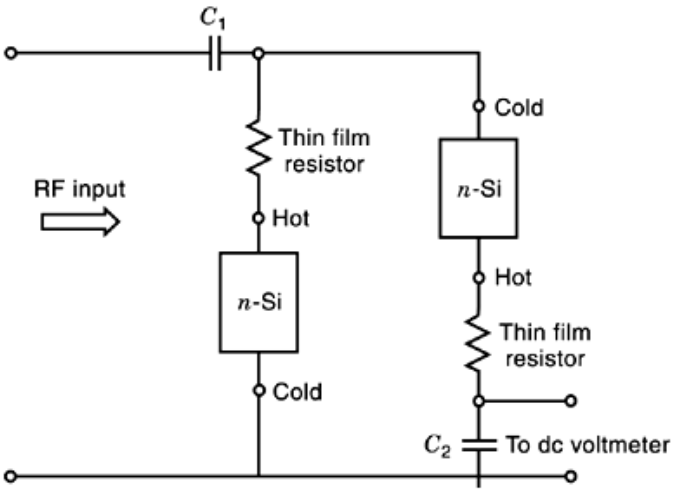

Fig. 19. Thermocouple power sensor.

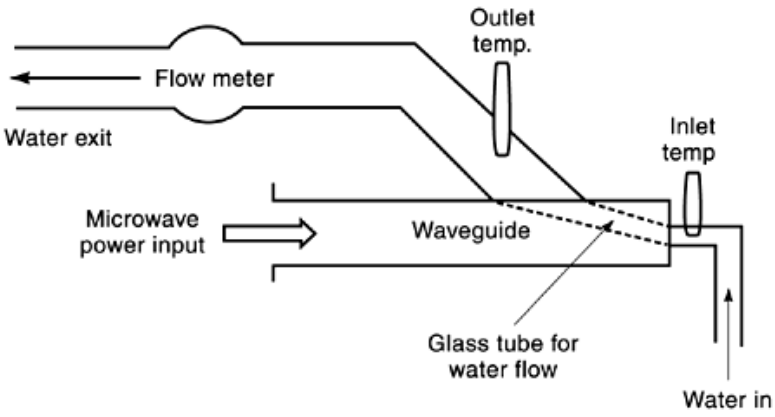

Fig. 20. Calorimetric flow measurement system.

BIBLIOGRAPHY

MICROWAVE RADIOMETRY

1. F. T. Ulaby R. K. Moore A. K. Fung *Microwave Remote Sensing: Active and Passive*, vols. 1–3, Reading, MA: Addison Wesley, 1981–1986.
2. C. Elachi *Introduction to the Physics and Techniques of Remote Sensing*, New York: Wiley, 1987.
3. M. A. Janssen (ed.) *Atmospheric Remote Sensing by Microwave Radiometry*, New York: Wiley, 1993.
4. G. Rees *The Remote Sensing Databook*, London: Cambridge Univ. Press, 1999.
5. S. Chandrashekhar *Radiative Transfer*, New York: Dover, 1960.
6. L. Tsang J. A. Kong R. T. Shin *Theory of Microwave Remote Sensing*, New York: Wiley-Interscience, 1985.
7. A. K. Fung *Microwave Scattering and Emission Models and Their Applications*, Boston: Artech House, 1994.
8. G. Evans C. W. McLeish *RF Radiometer Handbook*, Dedham, MA: Artech House, 1977.

9. N. Skou *Microwave Radiometer Systems: Design and Analysis*, Norwood, MA: Artech House, 1989.
10. D. V. Land Medical microwave radiometry and its clinical applications, *IEE Colloq. on Applications of Microwaves in Medicine*, 1995, pp. 2/1–2/5.
11. Y. Leroy et al. *Microwave Radiometry for Noninvasive Thermometry*, New York: Gordon and Breach, 1987.

MICROWAVE SPECTROSCOPY

12. C. H. Townes A. L. Schawlow *Microwave Spectroscopy*, New York: McGraw-Hill, 1955; New York: Dover, 1975.
13. W. Gordy R. L. Cook *Microwave Molecular Spectra*, New York: Wiley, 1984.
14. D. R. Johnson R. Pearson Spectroscopy, in D. Williams (ed.), *Methods of Experimental Physics*, Vol. 13B, New York: Academic Press, 1976, Chap. 4. 3.
15. R. D. Suenram A. M. Andrews Microwave spectroscopy, in F. B. Dunning and R. G. Hulet (eds.), *Atomic, Molecular, and Optical Physics: Atoms and Molecules* (*Experimental Methods in the Physical Sciences, vol. 29B)*, New York: Academic Press, 1996, Chap. 14.
16. M. A. Janssen (ed.) *Atmospheric Remote Sensing by Microwave Radiometry*, New York: Wiley, 1993.
17. R. L. Poynter H. M. Picket Submillimeter, millimeter, and microwave spectral line catalog, *Appl. Opt*., **24**: 2235–2240, 1985.
18. S. Y. Liao *Microwave Devices and Circuits*, 3rd ed., Englewood Cliffs, NJ: Prentice-Hall, 1990.

MEASUREMENT OF PERMITTIVITY AND PERMEABILITY

19. Arthur von Hippel *Dielectrics and Waves*, New York: Wiley, 1954: Boston: Artech House, 1995.
20. H. M. Altschuler Dielectric constant, in M. Sucher and J. Fox (eds.) *Handbook of Microwave Measurements*, 3rd ed., New York: Polytechnic Institute of Brooklyn, 1963.
21. M. N. Afsar J. R. Birch R. N. Clarke (edited by G. W. Chantry), The measurement of the properties of materials, *Proc. IEEE*, **74**: 183–199, Jan. 1986.
22. S. Robert A. von Hippel A new method of measuring dielectric constant and loss in the range of centimeter waves, *J. Appl. Phys.*, **17**: 610–616, 1946.
23. M. D. Deshpande et al. A new approach to estimate complex permittivity of dielectric materials at microwave frequencies using waveguide measurements, *IEEE Trans. Microw. Theory Tech.*, **45**: 359–366, 1997.
24. C. C. Courtney Time-domain measurement of the electromagnetic properties of materials, *IEEE Trans. Microw. Theory Tech.*, **46**: 517–522, 1998.
25. A. Nyshadham C. L. Sibbald S. S. Stuchly Permittivity measurement using open-ended sensors and reference liquid calibration—an uncertainty analysis, *IEEE Trans. Microw. Theory Tech.*, **40**: 305–314, 1992.
26. M. Nicolsson G. F. Ross Measurement of the intrinsic properties of materials by time-domain techniques, *IEEE Trans. Instrum. Meas*., **19**: 377–382, 1970.
27. H. M. Cronson Time-domain measurements of components and materials, in E. K. Miller (ed.), *Time-Domain Measurements in Electromagnetics*, New York: Van Nostrand Reinhold, 1986, Chap. 10.
28. M. C. Nuss J. Orenstein Terahertz time-domain spectroscopy, in G. Gruener (ed.), *Millimeter and Submillimeter Wave Spectroscopy of Solids*, Berlin: Springer-Verlag, 1998, pp. 7–50
29. R. A. Waldron *The Theory of Waveguides and Cavities*, London: Maclaren, 1967.
30. R. G. Carter Accuracy of microwave cavity perturbation measurements, *IEEE Trans. Microw.Theory Tech.*, **49**: 918–923, 2001.
31. M. A. Saed Measurement of the complex permittivity of low-loss planar microwave substrates using aperture-coupled microstrip resonators, *IEEE Trans. Microw. Theory Tech.*, **41**: 1343–1348, 1993.
32. L. Silber Intrinsic properties of ferrites, in M. Sucher and J. Fox, (eds.), *Handbook of Microwave Measurements*, 3rd ed., New York: Polytechnic Institute of Brooklyn, 1963, Chap. XV.
33. F. Kremer et al. The application of oversized cavities for millimetre-wave spectroscopy, in K. J. Button (ed.), *Infrared and Millimeter Waves*, vol. 11, Orlando, FL: Academic Press, 1984.

34. A. L. Cullen Millimeter-wave open-resonator techniques, in K. J. Button (ed.), *Infrared and Millimeter Waves*, vol. 10, Orlando, FL: Academic Press, 1983.
35. S. Aditya T Naveen An automated open resonator technique for measurement of extinction cross-section of single falling water drops over X-band, in*Progress in Electromagnetics Research*, PIER-8, EMW Publishing, 1994, pp. 161–171.
36. M. N. Afsar D. Hanyi A novel open-resonator system for precise measurement of permittivity and loss-tangent, *IEEE Trans. Instrum. Meas*., **50**: 402–405, 2001.
37. J. Musil F. Zacek *Microwave Measurements of Complex Permittivity by Free Space Methods and Their Applications*, Amsterdam: Elsevier, 1986.
38. D. K. Ghodgaonkar V. V. Varadan V. K. Varadan Free-space measurement of complex permittivity and complex permeability of magnetic materials at microwave frequencies, *IEEE Trans. Instrum. Meas.*, **39**: 387–394, 1990.
39. J. Munoz M. Rojo A. Parreno J. Margineda Automatic measurement of permittivity and permeability at microwave frequencies using normal and oblique free-wave incidence with focused beam, *IEEE Trans. Microw. Theory Tech.*, **47**: 886–892, 1998.

TIME-DOMAIN MEASUREMENTS

40. E. K. Miller (ed.) *Time-Domain Measurements in Electromagnetics*, New York: Van Nostrand Reinhold, 1986.
41. D. H. Auston Ultrafast Optoelectronics, in W. Kaiser (ed.), *Ultrashort Laser Pulses and Applications* (*Topics in Applied Physics*, vol. 60), 1st ed., Berlin: Springer-Verlag, 1988, pp. 183–233.
42. S. L. Huang et al. On-wafer photoconductive sampling of MMICs, *IEEE Trans. Microw. Theory Tech.*, **40**: 2312–2320, 1992.
43. *Time Domain Reflectometry Theory*, Agilent Technologies Application Note 1304–2, 1998.
44. J. R. Pressley G. D. Sower Instrumentation for time-domain measurements, in E. K. Miller (ed.), *Time-Domain Measurements in Electromagnetics*, New York: Van Nostrand Reinhold, 1986.
45. T. S. Laverghetta *Handbook of Microwave Testing*, Norwood, MA: Artech House, 1981.
46. P. I. Somlo J. D. Hunter *Microwave Impedance Measurement*, London: Peter Peregrinus, 1985 (Chap. 6, Time domain reflectometry).
47. M. C. Nuss J. Orenstein Terahertz time-domain spectroscopy, in G. Gruener (ed.), *Millimeter and Submillimeter Wave Spectroscopy of Solids*, Berlin: Springer-Verlag, 1998, pp. 7–50
48. D. R. Grischkowsky Optoelectronic characterization of transmission lines and waveguides by terahertz time-domain spectroscopy, *IEEE J. Selected Topics Quant. Electron*, **6**: 1122–1135, Dec. 2000.
49. S. L. Huang C. H. Lee H. L. A. Hung Real-time linear time-domain network analysis using picosecond photoconductive mixer and samples *IEEE Trans. Microw. Theory Tech.*, **43**: 1281–1289, 1995.

SWEPT FREQUENCY MEASUREMENT OF SCATTERING PARAMETERS

50. R. S. Elliot *An Introduction to Guided Waves and Microwave Circuits*, Upper Saddle River, NJ: Prentice-Hall, 1997.
51. R. E. Collin *Foundations for Microwave Engineering*, New York: McGraw-Hill, 1992.
52. P. C. Ely Swept frequency techniques, *Proc. IEEE*, **55**: 991–1001, June 1967.
53. *High frequency swept measurements*, Hewlett Packard Application Note No. 183.
54. I. Kneppo *Microwave Measurement by Comparison Methods*, New York: Elsevier Science, 1988.
55. R. B. Marks A multiline method for network analyser calibration, *IEEE Trans. Microw. Theory Tech.*, **39**: 1205–1215, 1991.
56. A. E. Bailey *Microwave Measurements*, London: Peter Peregrinus, 1985.
57. O. M. Caldwell J. D. Huff High speed error corrected vector *S*-parameter measurements, *IEEE Instrum. Meas. Technol. Conf.*, 1991, pp. 27–34.
58. R. Soares P. Gouzien P. Legaud Matching network characterization by *S*-parameter measurements of two port active devices, *Proc. IEE, Pt. H*, **135**: 426–430, 1988.

59. J. M. Mirande et al. Characterization of parasites in microwave device comparing *S* and noise parameter measurements with two different on wafer calibration techniques, *IEEE Instrum. Technol. Conf.*, 2001, pp. 530–533.
60. J. Hinojosa *S*-parameter broadband measurements on microstrip and fast extraction of the substrate and intrinsic properties, *IEEE Microw. Wireless Comp. Lett.*, **11**: 305–307, July 2001.

SIX-PORT REFLECTOMETERS

61. G. H. Engen Power equations: A new concept in the description and evaluation of microwave systems, *IEEE Trans. Microw. Theory Tech.*, **20**: 49–57, 1971.
62. C. A. Hoer A network analyser incorporating two six ports, *IEEE Trans. Microw. Theory Tech.*, **25**: 1070–1074, 1977.
63. G. F. Engen The six-port reflectometer: An alternative network analyser, *IEEE Trans. Microw. Theory Tech.*, **25**: 1075–1080, 1977.
64. G. F. Engen An improved circuit for implementing the six-port technique of microwave measurements, *IEEE Trans. Microw. Theory Tech.*, **25**: 1080–1083, 1977.
65. G. F. Engen C. A. Hoer 'Thru-reflect-line': An improved technique for calibrating the dual six-port automatic network analyzer, *IEEE Trans. Microw. Theory Tech.*, **27**: 987–993, 1979.
66. H. M. Cronson L. Susman A six-port automatic network analyzer, *IEEE Trans. Microw. Theory Tech.*, **25**: 1086–1091, 1979.
67. G. F. Engen *Microwave Circuit Theory and Foundations of Microwave Metrology*, London: Peregrinus, 1992.
68. S. Jia New application of a single six-port reflectometer, *Electron. Lett.*, **29**: 920–922, 1984.
69. F. Wiedmann et al. New structure for a six-port reflectometer in monolithic microwave integrated-circuit technology, *IEEE Trans. Instrum. Meas.*, **40**: 527–530, 1997.
70. S. P. Yeo M. Cheng New technique for measuring coefficients of two port devices, *Electron. Lett.*, **30**: 1951–1953, Nov.1994.
71. S. Khouaja F. M. Ghannouchi A single six-port based automated network analyser, *IEEE MTT Symp. Dig.*, 1503–1506, 1998.
72. M. E. Bialkowski Microwave network analyzer incorporating a single six-port reflectometer, *AEU Int. J. Electron. Commun.*, **40**: 197–199, 1986.
73. G. S. Woods M. E. Bialkowski Integrated design of an automatic six-port network analyzer, *Proc. IEE, Pt.H*, **137**: 67–74, 1990.
74. P. I. Somlo J. D. Hunter D. C. Arthur Accurate six-port operation with uncalibrated nonlinear diodes, *IEEE Trans. Microw. Theory Tech.*, **33**: 281–282, 1985.

POWER MEASUREMENTS

75. H. J. Carlin Measurement of power, in M. Sucher and J. Fox (eds.), *Handbook of Microwave Measurements*, New York: Polytechnic Institute of Brooklyn, 1963, Chap. III.
76. T. S. Laverghetta *Modern Microwave Measurements and Tehniques*, Norwood, MA: Artech House, 1988.
77. A. Y. Rumfelt L. B. Elwell Radio frequency power measurements, *Proc. IEEE*, **55**: 837–850, 1967.
78. A. E. Bailey *Microwave Measurements*, London: Peter Peregrinus, 1985.
79. L. Brunetti E. Monticone Standard power sensor in millimeter wave band, *Conf. on Precision Electromagnetic Measurements*, 1988, pp. 377–378.
80. IEEE Standard application guide for bolometric power meters, IEEE Std 470-1972, 27 Dec. 1972.
81. A. Fantom, *Radio Frequency and Microwave Power Measurement*, London: Peter Peregrinus, 1990.
82. B. Mellouet L. Velasco J. Achkar Fast method applied to the measurement of microwave power standards, *IEEE Trans. Instrum. Meas.*, **50**: 381–384, 2001.
83. T. S. Laverghetta *Modern Microwave Measurements and Techniques*, Artech House, Norwood, MA, 1988.
84. N. P. Abbott C. J. Reeves G. R. Orford A new waveguide flow calorimeter for levels 1–20 W, *IEEE Trans. Instrum. Meas.*, **23**: 414–420, 1974.

85. N. S. Chung et al. Coaxial and waveguide microcalorimeters for RF and microwave power standards, *IEEE Trans. Instrum. Meas.*, **38**: 460–469, 1989.

SHEEL ADITYA
ALPHONES AROKIASWAMI
Nanyang Technological University